Full Length Research Paper

Numerical investigation of axial bearing capacity of piles embedded in sloping ground

Abbas Babaei

Department of Civil Engineering, Noor Branch, Islamic Azad University, Noor, Iran. E-mail: a_babaei@iaunour.ac.ir/
abbas.babaee11@gmail.com.

In practice, piles may be constructed in sloping ground where the axial capacity of piles may be affected by the ground slope. This paper presents the effect of the ground slope geometry on the ultimate axial bearing capacity of vertical pile using numerical simulation based on Plaxis 3D Foundation software. The pile is assumed to consist of linear and elastic material. Various aspect ratios (L/D) for the pile have been considered. The soil behavior is modeled based on the Mohr Coulomb failure criterion. Loose and dense sand, and sandy clay have been used for numerical modeling. Interface elements have been applied to the pile-soil boundaries to accommodate the slip which may occur between these two materials. The simulation of the pile-soil system is first calibrated using available data from the field load tests on piles to ensure the validity of the constructed numerical modeling. Various shapes for the ground slope have been considered in analyses, including flat-sloping, uniformly sloping, all-around upward sloping, and all-around downward sloping ground. The results have shown that the pile axial capacity increases with increase in the value of the upward sloping. In contrast, the pile capacity decreases with increase in the downward sloping. From a provided data base, empirical expressions have been presented to take into account the slope shape effect on the pile capacity. It has been found that this empirical expression can be confidently used in practice to account for the ground sloping effect on the pile capacity. This expression may be used in conjunction with conventional methods based on the limit equilibrium approach. This is interesting since practicing engineers are well familiar with conventional methods calculating the pile axial capacity.

Key words: Pile, ground slope, axial capacity, pile, Mohr Coulomb, numerical method, finite element, Mohr Coulomb failure criterion.

INTRODUCTION

Piles are structural components made of wood, concrete or steel and are used for transferring of surface loads to ground depth. The expenditure of pile set-up is much higher than shallow foundations. Despite this, in practice, they are still widely used for sufficient capacity and low settlement requirements. The subject of load-carrying capacity of piles has been extensively investigated using numerical, analytical or experimental methods (Donald, 2000; Kim and Barker, 2010). However, the ground sloping effect on pile response under axial loading has not been explored, to the best knowledge of the authors.

In this paper, numerical simulation based on Plaxis 3D Foundation has been used to determine the influence of the ground slope on the pile axial capacity. Based on the numerical results, empirical expressions have been introduced which may be used in conjunction with conventional methods to compute the bearing capacity of piles embedded in sloping ground (Bowles, 2001).

Axial bearing capacity of piles

Various methods may be used to calculate the axial

capacity of piles due to the failure of the soil around the pile shaft and toe. These include static analysis, using *in-situ* tests, dynamic method, and direct load test. In static analysis, shear strength parameters of the soil is used in conventional approaches. Total or effective stress analyses may be used in this method. As a complementary method, *in-situ* test results may also be used which provide continuous information of the site soil (Titi et al., 1999; Eslami and Fellenius, 1997). Dynamic methods are on the base of the relation between the exerting energy and pile reaction or emitted wave equation analysis of pile during the pile embedment. During loading test, the pile exposes a static load in the real condition and its load-displacement characteristics are studied at different states. As a result, the pile capacity stemming from shaft and toe resistance components are obtained. This is partially lengthy, difficult, and expensive; however, it can be directly evaluating the pile capacity. Numerical approaches are useful and powerful tools to deal with complexity of the pile problems (Budhu, 2010).

Numerical simulation of pile-soil system

To calculate the axial capacity of pile subjected to vertical load, the final element program $Plaxis\,^{3D}\,Foundation$ has been used. This program has capability to model the soil-structure interaction and considers precisely the soil and structure behavior with no simplification. The finite element mesh is extended to the boundaries around the pile sufficiently to avoid unrealistic results. The lateral boundary was assumed to be at 5r where r denotes the pile radius. The soil behavior is assumed to obey the Mohr-Coulomb failure criterion.

Verification

To demonstrate the capability of the constructed numerical soil-pile simulation, field test data reported in the literature are considered. First, data are reported by Ismael (2001, 1990, and 1996), Ismael and Sanad (1993), Ismael et al. (1994) and the second tests were performed by Neves et al. (2001) and third tests were performed by El-Mossallamy (1999).

Tensile loading calibration

Ismael (2001) performed field tension loading test site South Surra on a real full scale pile. The soil profile in the site is shown in Figures 1, 2 and 3. The specifications of the soil and pile are given in Table 1.

Compressive calibration model in non homogenous soil

In the second test, a test pile embedded in an inhomogeneous soil is considered. The soil and pile specifications are given in Figures 4, 5 and 6 and Table 2.

Compressive calibration model in homogenous soil

Two cases showed that the predictions made by numerical analyses are reasonable and can be used confidently to simulate soil-pile in sloping ground (Figures 7, 8 and 9).

Numerical simulation of soil-pile system in sloping ground

To explore the slope effect on the pile axial capacity, six slope geometries are considered and the pile capacity is compared with the same pile embedded into a flat ground of the same properties (Figure 10). For this purpose, loose sand and three slenderness ratios of 30, 40, and 50 are used. The pile diameter is assumed 1 m in all analyses. The soil and pile properties are given in Table 3.

Result in five geometrical slope state while L/D=30, 40 and 50

Here, the results for slope geometries (a, b, c, e, and f) with the pile slenderness ratios of L/D=30, 40 and 50 are presented. Figures 11, 12 and 13 show the axial capacity ratio versus the ground slope. This ratio represents the axial capacity of the pile embedded into a sloping ground divided by the axial capacity of the same pile embedded into the horizontal ground of the same properties. Each figure corresponds to a slenderness ratio. As seen in each figure, the pile capacity increases with increase in the lateral pressure due to the ground slope on the pile shaft. It is also noted that, in some cases, there is a decrease in the axial capacity of the pile.

  Based on the results presented in Figures 11, 12 and 13, the following empirical expression is presented:

$$\frac{\Delta Q_{ult-\beta}}{Q_{ult-(\beta=0)}} = \frac{1}{100}\alpha\beta$$

(1)

Where Q_{ult} represents the pile axial capacity increment and Q_{ult} denotes the axial capacity of the same pile embedded into the horizontal ground of the same properties. Character expresses the ground surface
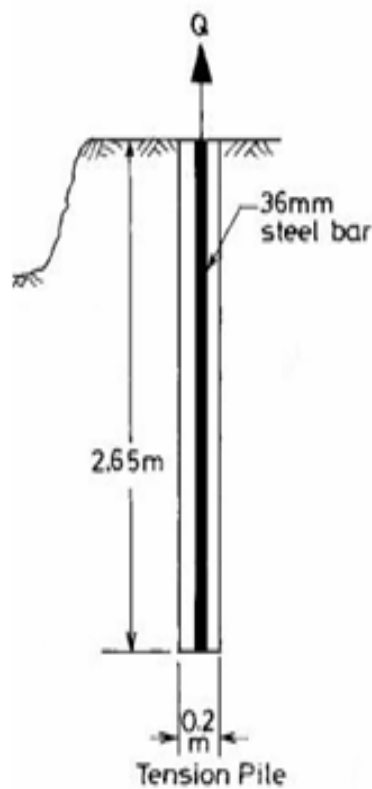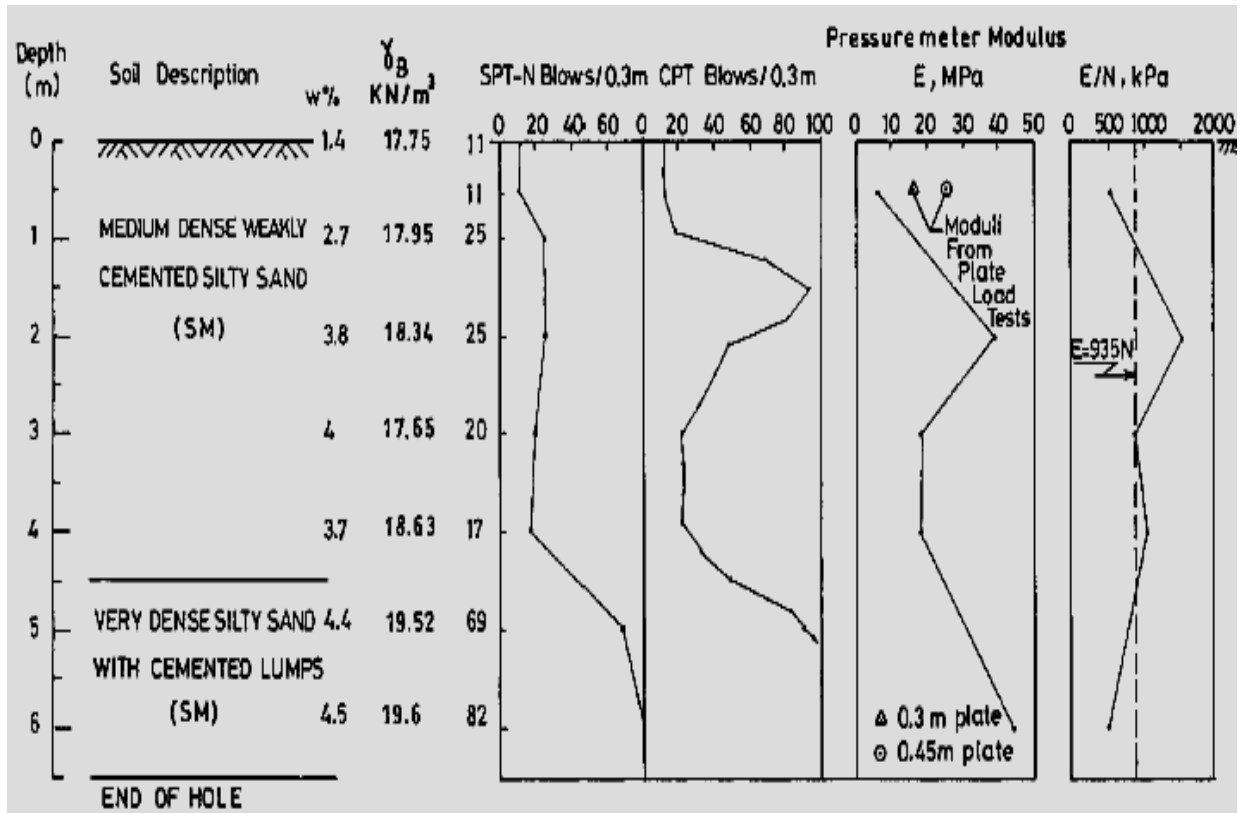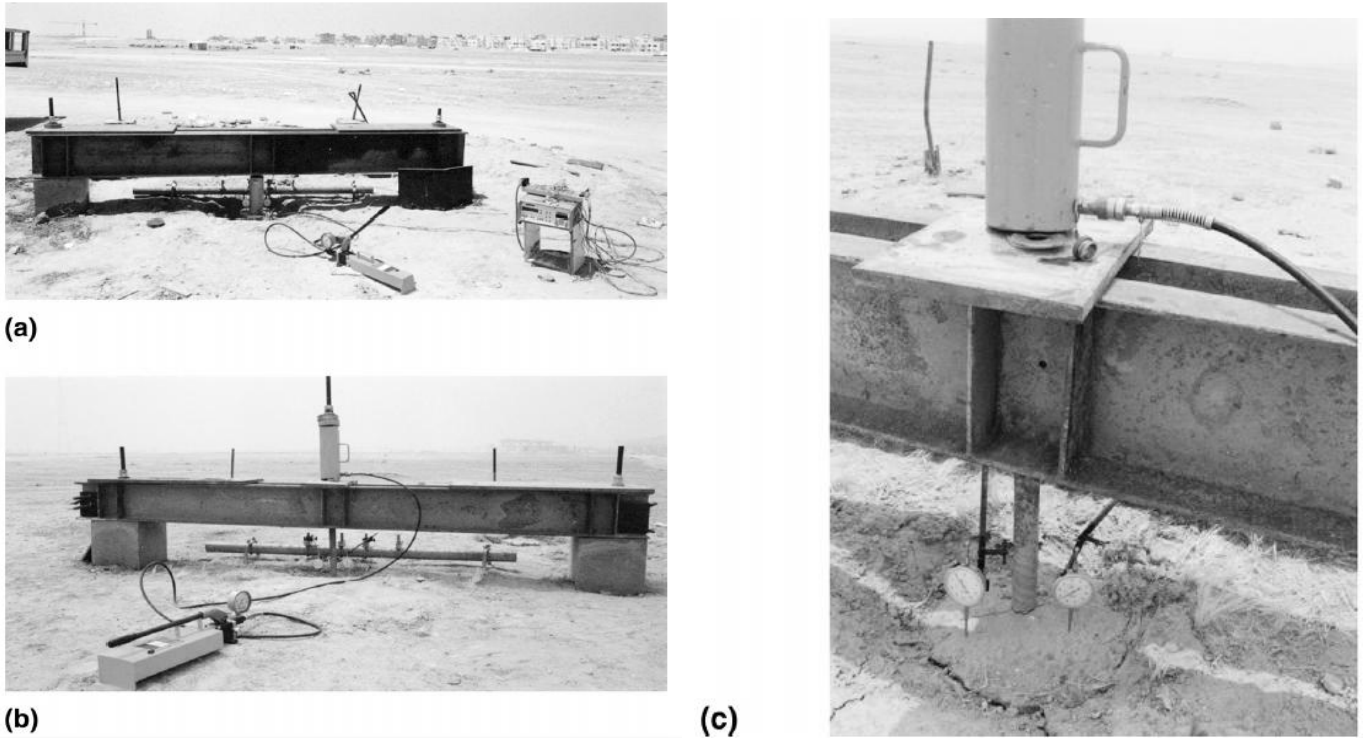
Figure 1. Soil conditions at test site South Surra.

Figure 2. (a) set-up for test; (b) tensile test; (c) pile fracture after tension Ismael (2001).
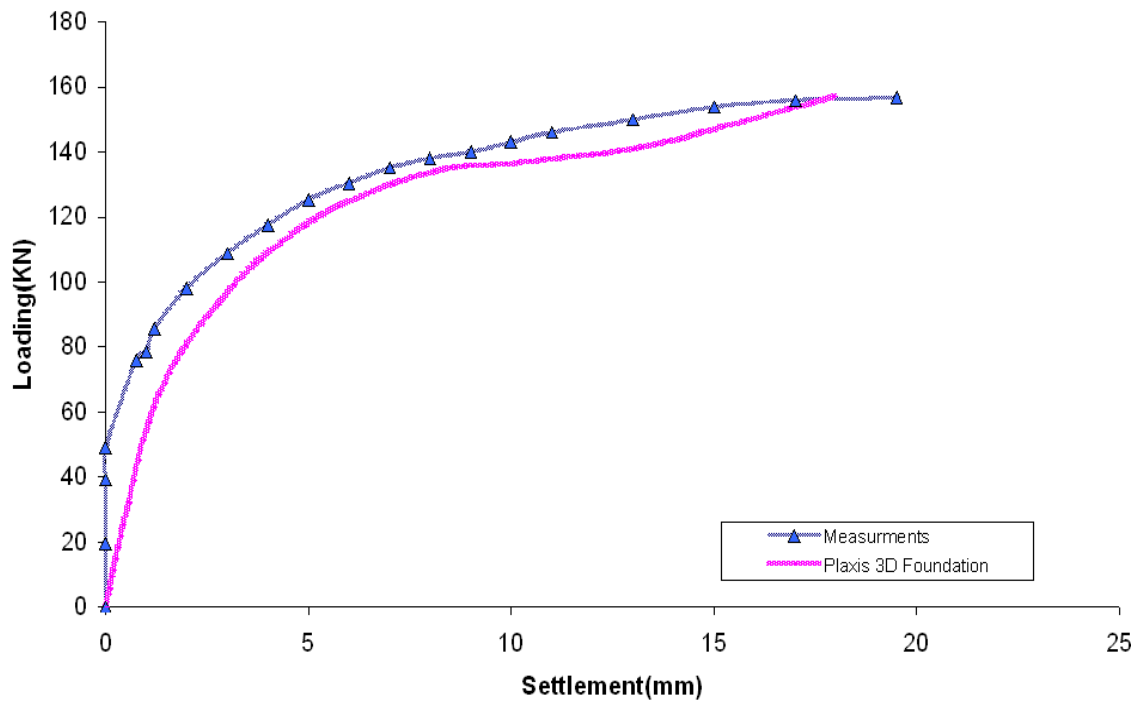

Figure 3. Comparison between measured data reported by Ismael (2001) and predicted data by Plaxis 3D for pile with diameter 0.2 m.

Table 1. Soil and pile properties for numerical simulation (LE: Linear Elastic, MC: Mohr Coulumb).

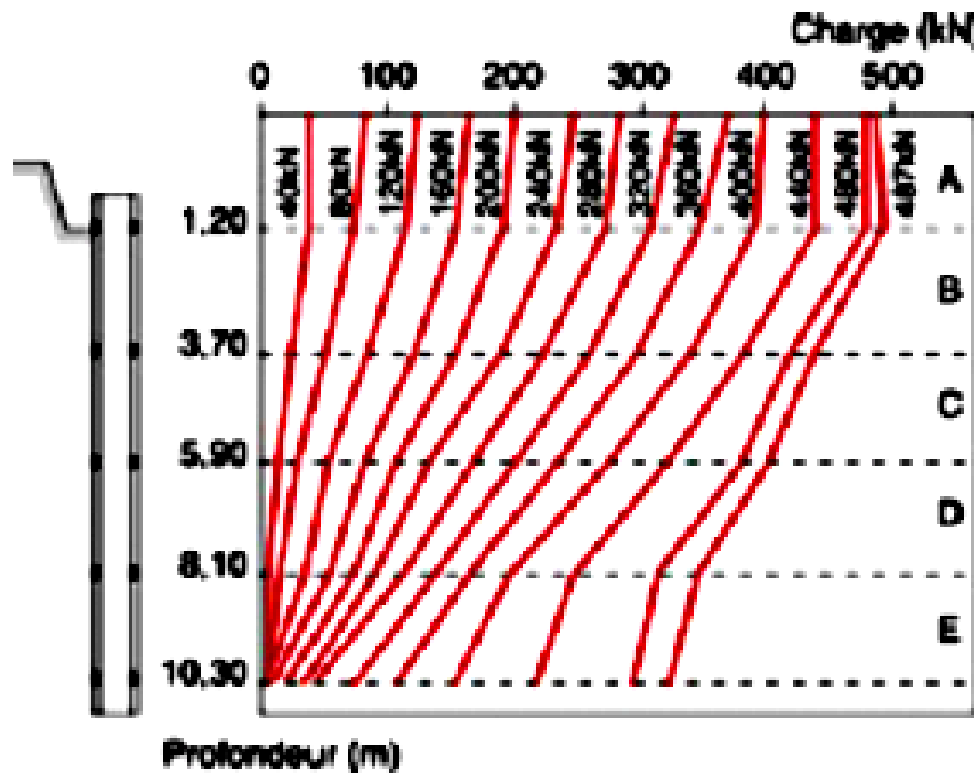| Property	Layer 1	Layer 2	Pile
Model	MC	MC	LE
$\gamma_{satt}(kN/m^3)$	18	19.6	23
$\gamma_{unsat}(kN/m^3)$	18	19.6	-
$E(MN/m^2)$	37	40	32000
ν	0.3	0.3	0.3
$c(kN/m^2)$	20	20	-
$\phi(\circ)$	35	35	-
$\psi(\circ)$	0	0	-
R_{inter}	1	1	1
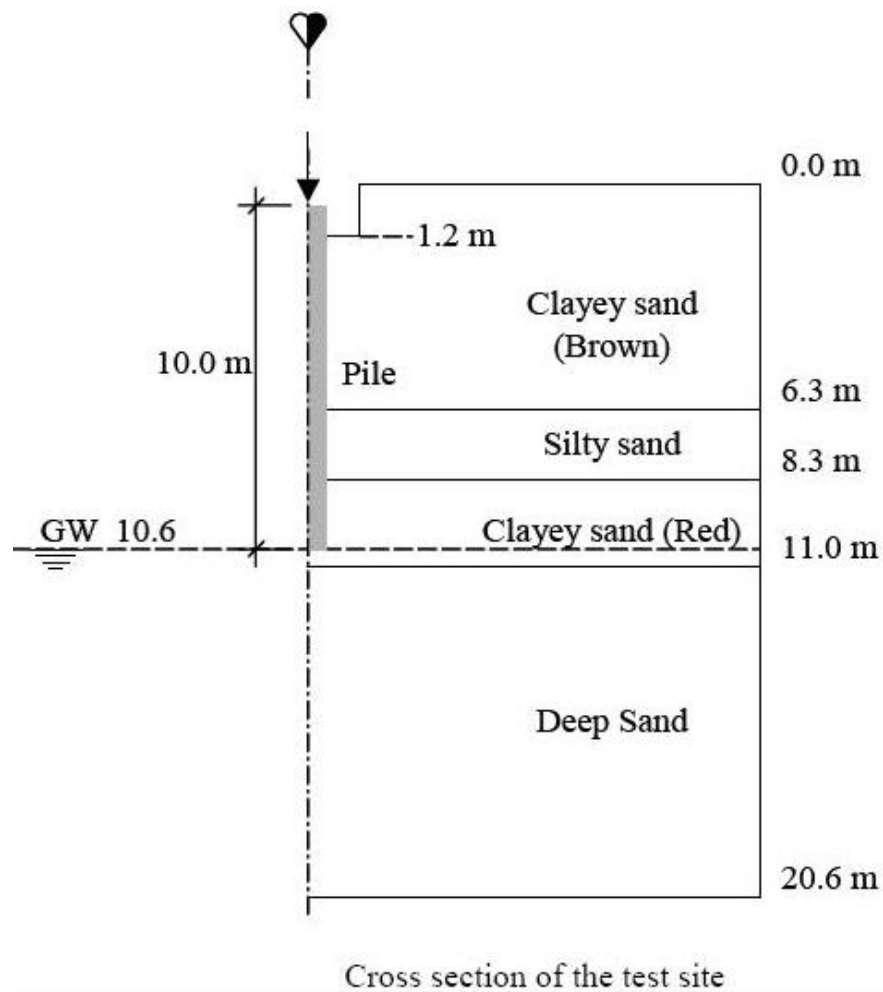
Figure 4. Soil profile at Saopaolo University Campus (Neves et al., 2001).

b. 0.40 m diameter pile

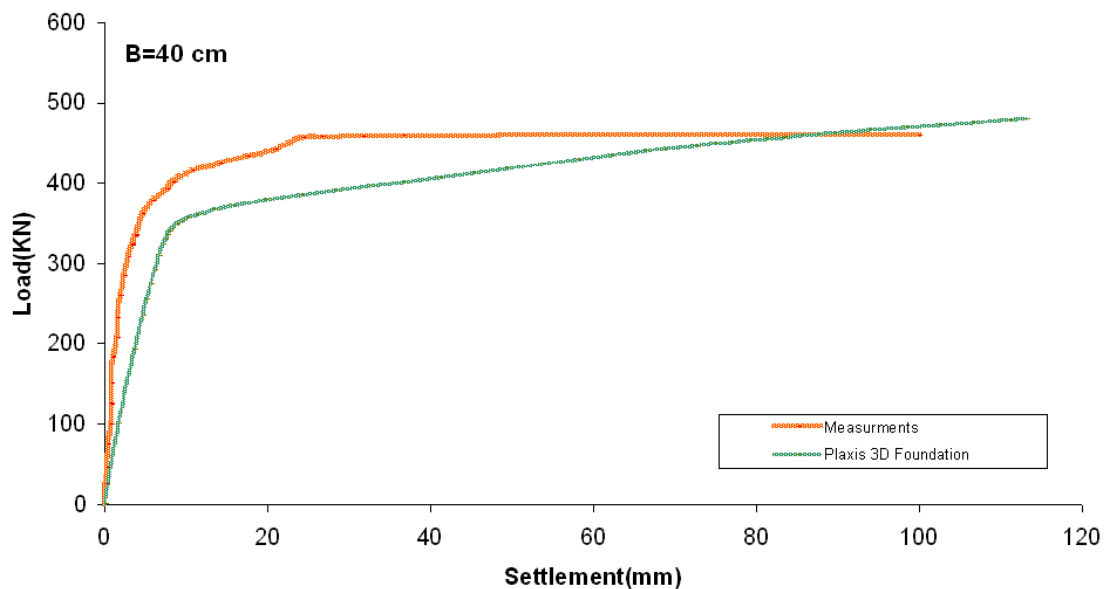**Figure 5.** Load distribution along the loaded pile (Neves et al., 2001).

Figure 6. Comparison between measured data.

Table 2. Soil and pile specifications used in numerical simulation.

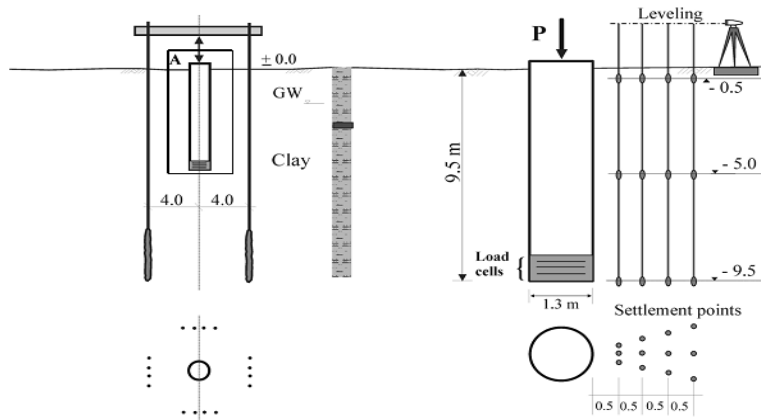| Property	Layer 1	Layer 2	Layer 3	Layer 4	Pile
Model	MC	MC	MC	MC	LE
$\gamma_{sat}(kN/m^3)$	16.7	18.8	19.8	19.8	24
$\gamma_{unsat}(kN/m^3)$	16.7	18.8	19.8	19.8	-
$E(MN/m^2)$	9.15	13.51	13.57	19.3	29200
v	0.12	0.12	0.07	0.05	0.3
c (kN/m^2)	13	12	14	17	-
$\phi(\circ)$	26	23	23	23	-
$\psi(\circ)$	0	0	0	0	-
R_{inter}	1	1	1	1	1

Figure 7. Layout of the pile load test and the measurement points (El-Mossallamy, 1999).
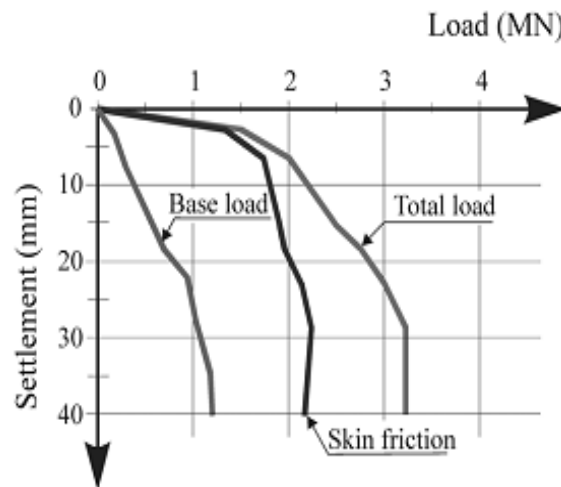

Figure 8. Measured load-settlement curves and distribution of loads between base resistance and skin friction (El-Mossallamy, 1999).
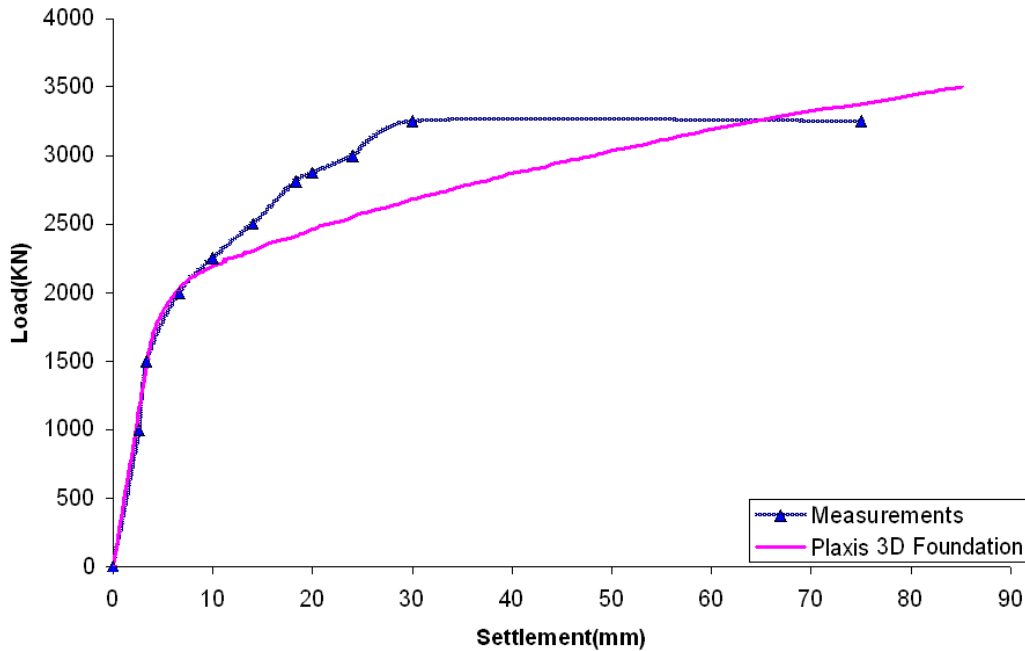
Figure 9. Comparison between measured data reported by El-Mossallamy (1999) and predicted data by Plaxis 3D for pile with diameter 1.3 m.

slope angle.

Table 5 presents the values of used in Equation 1. The positive values show an n increase in pile capacity and negative values correspond to a decrease in the axial pile capacity.

Limit equilibrium methods

In practice, the axial pile capacity is determined using limit equilibrium relationships introduced, for example by Vesic (1977) and Kulhawy and Mayne (1990), etc. Table 6 offers pile axial capacity computed by these methods. The extra lateral pressure exerted to the pile due to the sloping ground may be evaluated using Boussinesqe method (1885) (Budhu (2010). This method gives the lateral pressure due to surcharges using the elasticity theory and assuming semi-infinite, homogenous and elastic soil. Figure 14 shows the pressure due to a triangular load. At a given depth of z, the pressure on a retaining wall is estimated using:

$$\sigma_h(z) = \frac{q}{\pi}(\frac{x}{B}\alpha - \frac{z}{B}\ln\frac{R_1^2}{R_2^2} + \frac{1}{2}\sin 2\beta)$$

(2)

$$R_1 = \frac{z}{\cos(\beta+\alpha)}$$

(3)

$$R_2 = \frac{z}{\cos\beta}$$

(4)

$$\alpha = \tan^{-1}\frac{x}{z}$$

(5)

$$\beta = \tan^{-1}\frac{B+x}{z} - \alpha$$

(6)

The lateral force yielding from the slope with geometry b (Table 4) is obtained using Boussinesqe method shown in Figure 14. The axial capacity of the pile embedded into a horizontal ground is first computed. For the additional load exerted to the pile shaft due to the ground slope, the lateral force is computed using Boussinesqe method and then it is multiplied by $\tan\delta$. This gives $P_{(z)}.\tan\delta$, where $P_{(z)}$ is the additional horizontal excess load due to the surcharge and δ is the friction angle between the soil and the pile material. The following equation gives the ultimate axial load carried by the pile:

$$Q_{total} = Q_{ult(K)} + P_{(z)}.\tan\delta$$

(7)

Where Q_{total} represents the ultimate axial load carried by the pile in sloping ground, Q_{ult} .the ultimate pile capacity
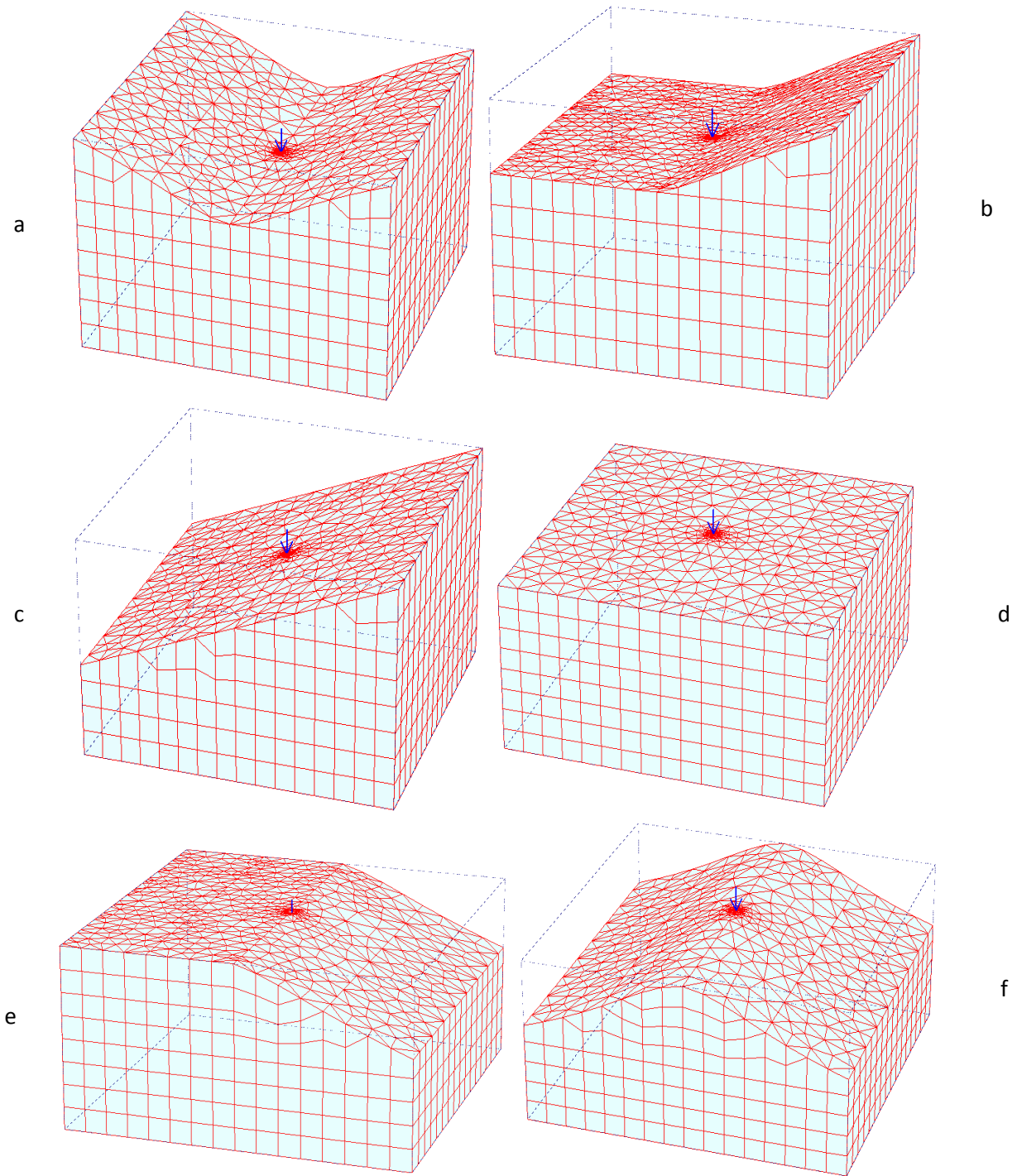
**Figure 10.** Various ground geometry used for numerical simulation.

in horizontal ground, and $P_{(z)}$ tanδ denotes the additional load carried by the pile due to the sloping ground. Character K stands for Kulhawy and Mayne (1990). Table

6 compares the results obtained from Equation 7 and Plaxis 3D.

Considering Tables 6 to 9 and Figures 15 and 16, it

Table 3. Soil and pile specifications used in numerical simulation.

Property	Soil	Pile
Model	MC	LE
$\gamma_{satt}(KN/m^3)$	20	24
$\gamma_{unsat}(KN/m^3)$	20	-
$E(MN/m^2)$	60	30000
ν	0.3	0.2
$c(KN/m^2)$	20	-
$\phi(\circ)$	22.5	-
$\psi(\circ)$	0	-
R_{inter}	1	1
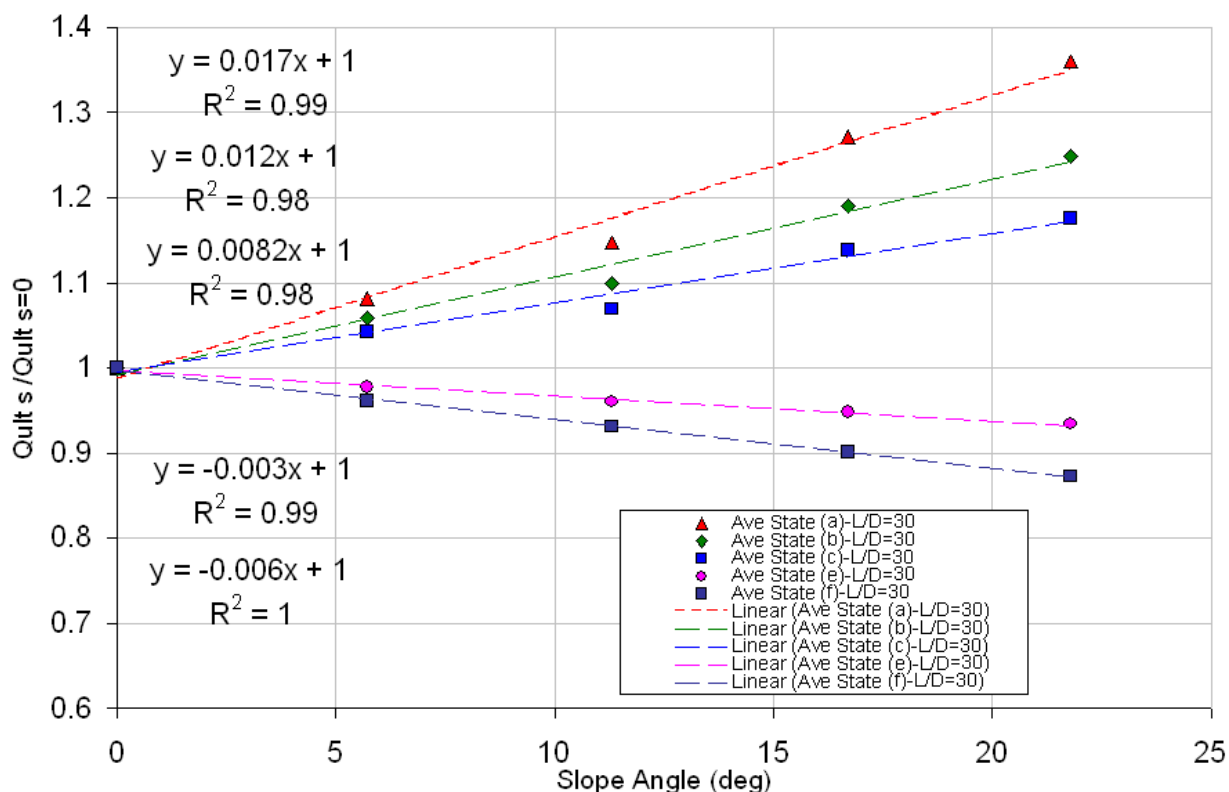
Figure 11. Load ratio versus the slope angle for L/D=30 for various sloping ground (cases a, b, c, e, f).

may be concluded that there is generally a good agreement between results obtained from Plaxis 3D and conventional methods in conjunction with Equation 7 for determination of axial capacity of piles embedded in sloping ground.

CONCLUSIONS

In this paper, the effect of slope on axial bearing capacity of vertical piles by using Plaxis 3D Foundation has been investigated. For modeling Fine meshes has been used
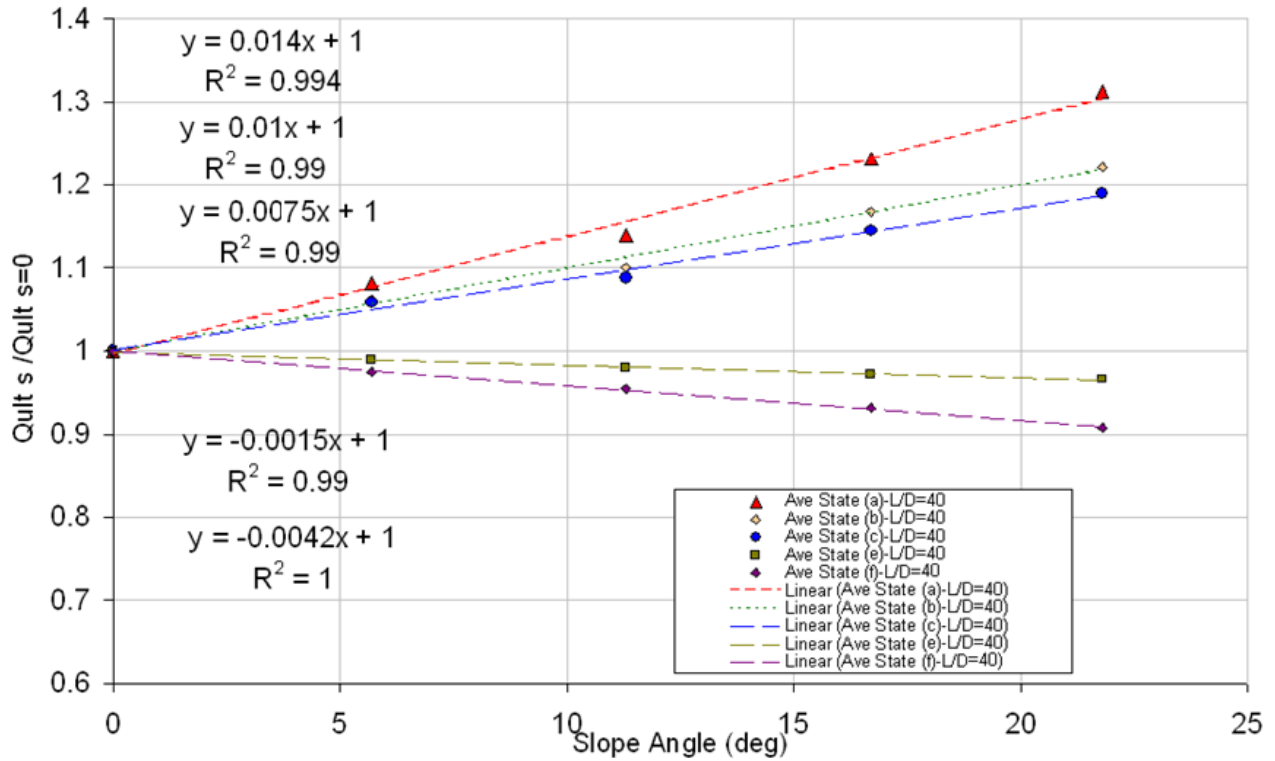
Figure 12. Load ratio versus the slope angle for L/D=40 for various sloping ground (cases a, b, c, e, f).
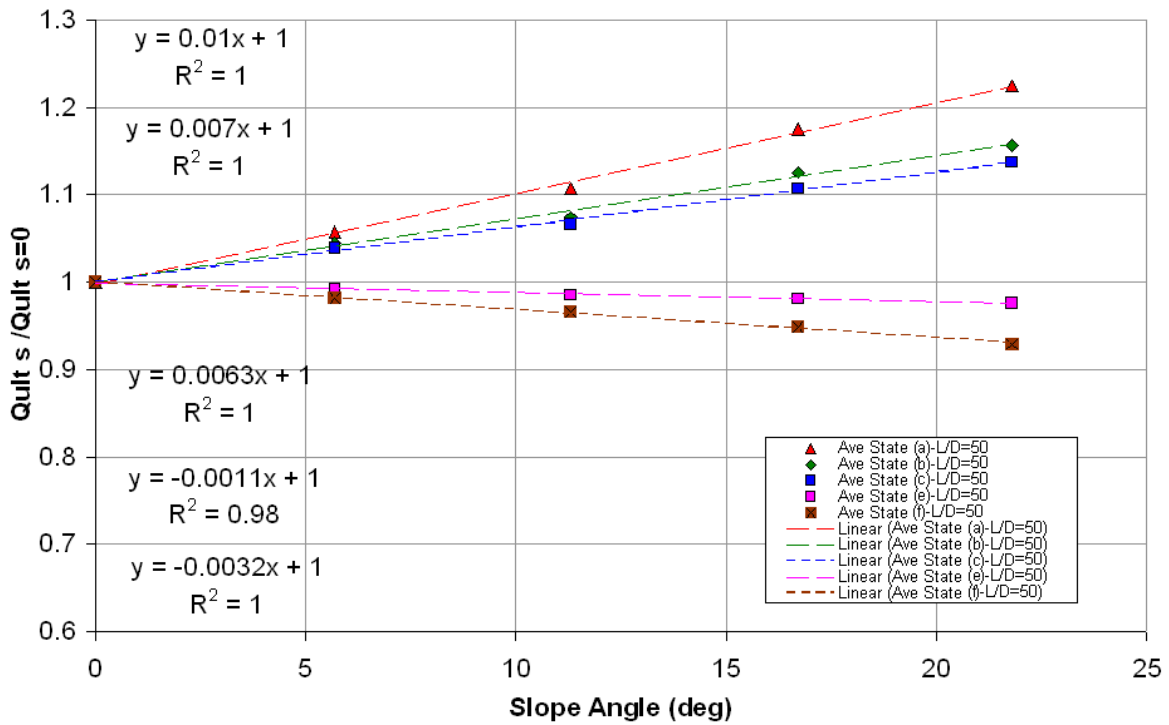

Figure 13. Load ratio versus the slope angle for L/D=50 for various sloping ground (cases a, b, c, e, f).

Table 4. Soil and pile properties used for numerical analyses of piles in sloping ground.

Property	Dense	Loose	Clay	Pile
Model	MC	MC	MC	LE
$\gamma_{satt}(kN/m^3)$	20	20	20	**24**
$\gamma_{unsat}(kN/m^3)$	17	17	**20**	-
$E(MN/m^2)$	105	**45**	**60**	29200
ν	0.3	0.3	0.3	0.3
$c(kN/m^2)$	**1**	**1**	20	-
$\phi(\circ)$	35	**35**	22.5	-
$\psi(\circ)$	**5**	**5**	**0**	-
R_{inter}	**1**	**1**	**1**	**1**

Table 5. Values of used in Equation (1) for L/D=30, 40, and 50.

State slope	Slope geometry	L/D=30	L/D=40	L/D=50
a		1.7	1.4	1.0
b		1.2	1.0	0.7
c		0.82	0.75	0.63
e		-0.3	-0.15	-0.11
f		-0.6	-0.42	-0.32

Table 6. Pile axial capacity calculated from conventional limit equilibrium method.

| L/D	Soil type	Toe bearing load Based on Vesic method (kN) (I)	Toe bearing load based on Kulhawy method (kN) (II)	Shaft resistance β-method $L' = 15D$ (kN) (J)	Total load (kN) (I+J)	Total II&J (kN) (II+J)	Axial capacity based on Plaxis 3D (10%D) (kN)
30	Loose	11680	16317	5407	17087	21724	19665
30	Dense	14113	20116	5407	19520	25523	28080
30	Clay	5263	6714	7398	12661	14112	10026
40	Loose	13239	18704	7811	21050	26515	26250
40	Dense	16548	23423	7811	24359	31234	37125
40	Clay	6230	7039	10477	16707	17516	15400
50	Loose	14883	21236	10214	25097	31450	30720
50	Dense	18605	26226	10214	28819	36440	42450
50	Clay	9260	10304	13556	22816	23860	20672
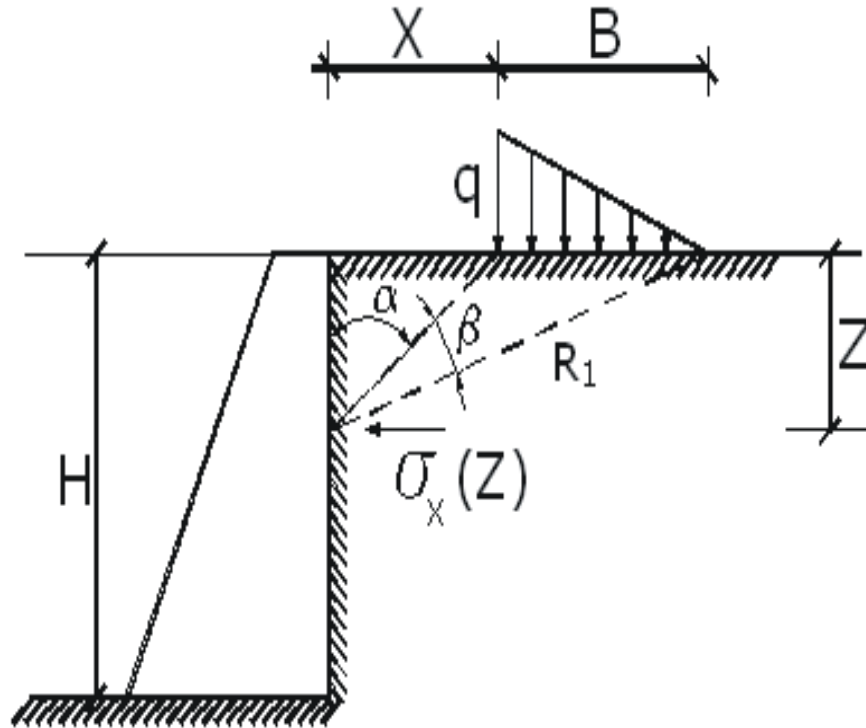
Figure 14. Lateral pressure induced to the wall due to triangular surcharge.

Table 7. Comparison of pile axial capacity determined from Plaxis 3D and limit equilibrium method for L/D=30.

β	$P_{(z)_\beta}$ (kN)	$P_{(z)_\beta}.\tan\delta$ (kN)	$Q_{ult(V)_{\beta=0}} + P_{(z)_\beta}.\tan\delta$ (kN)	$Q_{ult(K)_{\beta=0}} + P_{(z)_\beta}.\tan\delta$ (kN)	$Q_{ult(Plaxis.3D.F)}$ (kN)
21.8°	3157.7	2211.0	19298	23935	22950
16.7°	2368.3	1658.3	18745	23382	22095
11.31°	1578.9	1105.6	18192	22830	20880
5.7°	789.4	552.7	17640	22277	20250
0.0°	0.00	0.00	17087	21724	19665

(Note: K and V stand for Kulhawy and Vesic, respectively).

Table 8. Comparison of pile axial capacity determined from Plaxis 3D and limit equilibrium method for L/D=40.

β	$P_{(z)_\beta}$ (kN)	$P_{(z)_\beta}.\tan\delta$ (kN)	$Q_{ult(V)_{\beta=0}} + P_{(z)_\beta}.\tan\delta$ (kN)	$Q_{ult(K)_{\beta=0}} + P_{(z)_\beta}.\tan\delta$ (kN)	$Q_{ult(Plaxis.3D.F)}$ (kN)
21.8°	5725	4009	25059	30524	29325
16.7°	4294	3007	24057	29522	28575
11.31°	2863	2005	23055	28520	27600
5.7°	1431	1002	22052	27517	26925
0.0°	0.00	0.00	21050	26515	26250

Table 9. Comparison of pile axial capacity determined from Plaxis 3D and limit equilibrium method for L/D=50.

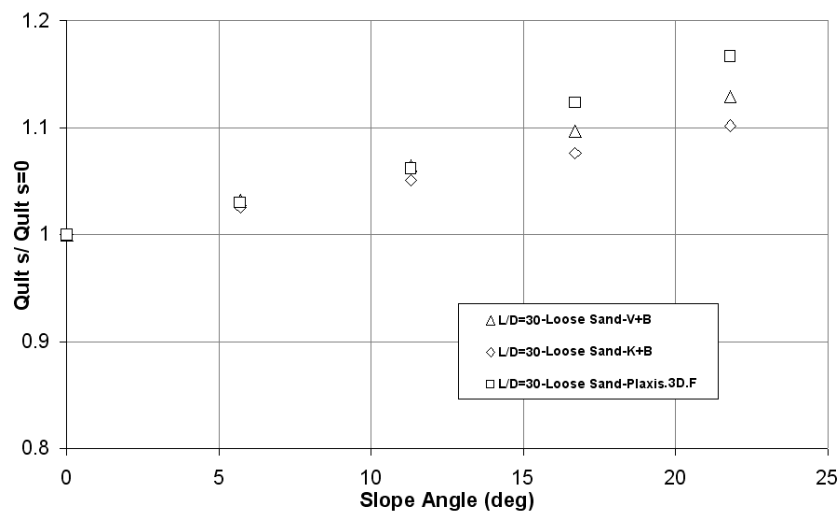| β	$P_{(z)_\beta}$ (kN)	$P_{(z)_\beta}.tag(\delta)$ (kN)	$Q_{ult(V)_{\beta=0}}+P_{(z)_\beta}.tag(\delta)$ (kN)	$Q_{ult(K)_{\beta=0}}+P_{(z)_\beta}.tag(\delta)$ (kN)	$Q_{ult(Plaxis.3D.F)}$ (kN)
21.8°	7842	5491	30588	36941	33360
16.7°	5882	4119	29216	35569	32940
11.31°	3921	2746	27843	34196	32040
5.7°	1961	1373	26470	32823	31380
0.0°	0.00	0.00	25097	31450	30720

Figure 15. Comparison of pile axial capacity ratio determined from Plaxis 3D and limit equilibrium methods for L/D=30.
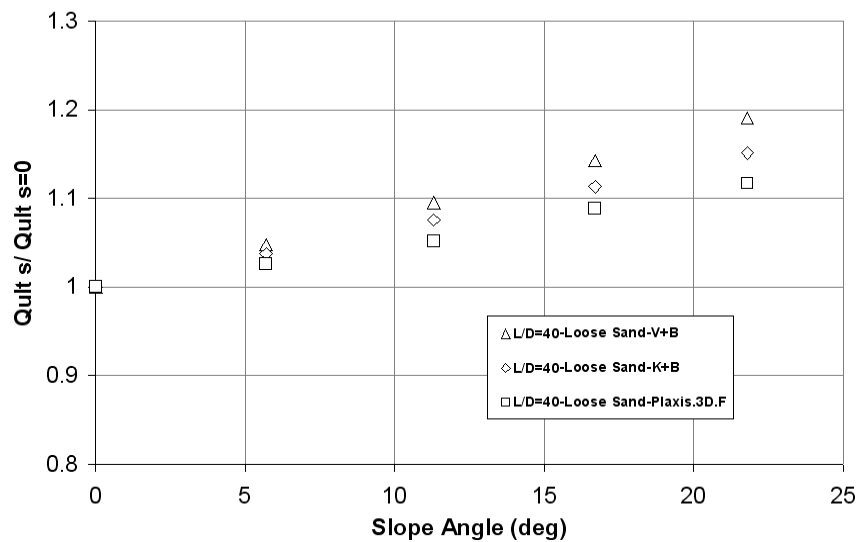

Figure 16. Comparison of pile axial capacity ratio determined from Plaxis 3D and limit equilibrium methods for L/D=40.

and to eliminate the sensitivity to meshing, at a distance of five times of pile radius around the pile finer meshes used. The investigations show the following results in loose and dense sands around medium to tall piles at common and stable slopes. The results have shown that the pile axial capacity increases with increase in the value of the upward sloping. In contrast, the pile capacity decreases with increase in the downward sloping.

REFERENCES

Bowles JE (2001) Foundation Analysis and Design. McGraw-Hill Press.

Donald PC (2000). Foundation Design: Principles and Practices. 2th Edition, Prentice Hall Press.

El-Mossallamy Y (1999). Load-settlement Behavior of Large Diameter Bored Piles in Over-Consolidated Clay. Proceeding of The 7th International Symposium on Numerical Models in Geotechnical Engineering, Graz, Austria. pp. 443-450.

Eslami AE, Fellenius BH (1997). Pile capacity by direct CPT and CPTu methods applied to 102 case histories. Canadian Geotech. J., 34(6): 886-904.

Titi HH, Murad Y, Abu-Farsakh (1999). Evaluation of Bearing Capacity of Piles from Cone Penetration Test Data. Louisiana Department of Transportation and Development Louisiana Transportation Research Center. Available at Online: http://www.vulcanhammer.info/drivability/Titi-Abu-Farsakh.pdf.

Ismael NF (1990). ''Behavior of laterally loaded bored piles in cemented sands.'' J. Geotech. Engrg. ASCE, 116(11): 1678–1699.

Ismael NF (1996). ''Loading tests on circular and ring plates in very dense cemented sands.'' J. Geotech. Engrg., ASCE, 122(4): 281–287.

Ismael NF, Al-Sanad HA, Al-Otaibi F (1994). ''Tension tests on bored piles in cemented desert sands.'' Can. Geotech. J., Ottawa, 31(3): 597–603.

Ismael NF, Al-Sanad HA (1993). ''Plate loading tests on weakly cemented surface desert sands.'' Geotech. Engrg., J. Southeast Asian Geotech. Soc., Bangkok, Thailand, 24(2): 133–150.

Ismael NF (2001). Axial Load Test Bored Piles and Pile Groups in Cemented Sands. J. Geotech. Geonviron. Eng., 127(9): 766-773.

Kim JS, Barker RM (2002). Effect of Live Load Surcharge on Retaining Walls and Abutments. J. Geotechnical and Geoenviromental Eng., 128(10): 803-812.

Kulhawy FH, Mayne PW (1990). Manual on estimating soil properties for foundation design. Report EL-6800, Electric Power Research Inst., Palo Alto, p. 306.

Budhu M (2010). Soil Mechanics and Foundations. 3th Edition, Wiley Press. 761p.

Neves M, Mestat P, Frank R, Degny E (2001). "Research on the behavior of bored piles - I. in situ and laboratory experiments", CESAR-LCPC, 231: 39-54.

Vesic AS (1977). Design of pile foundations. National Cooperative Highway Research Program Synthesis of Highway Practice No. 42, Transportation Research Board, National Research Council, Washington, D.C, pp. 24-26.